OMI total bromine monoxide (OMBRO) data product: Algorithm, retrieval and measurement comparisons

Raid M. Suleiman[1], Kelly Chance[1], Xiong Liu[1], Gonzalo González Abad[1], Thomas P. Kurosu[2], Francois Hendrick[3], and Nicolas Theys[3]

[1]Harvard-Smithsonian Center for Astrophysics, Cambridge, MA, USA
[2]Jet Propulsion Laboratory, California Institute of Technology, Pasadena, CA, USA
[3]Royal Belgian Institute for Space Aeronomy, Brussels, Belgium

Correspondence to: Raid M. Suleiman (rsuleiman@cfa.harvard.edu)

Abstract. This paper presents the retrieval algorithm for the operational Ozone Monitoring Instrument (OMI) total bromine monoxide (BrO) data product (OMBRO) developed at the Smithsonian Astrophysical Observatory (SAO), and shows comparisons with correlative measurements and retrieval results. The algorithm is based on direct nonlinear least squares fitting of radiances from the spectral range 319.0-347.5 nm. Radiances are modeled from the solar irradiance, attenuated by contributions from BrO and interfering gases, and including rotational Raman scattering, additive and multiplicative closure polynomials, correction for Nyquist undersampling, and the average fitting residual spectrum. The retrieval uses albedo and wavelength-dependent air mass factors (AMFs), which have been pre-computed using a single mostly stratospheric BrO profile. The BrO cross sections are multiplied by the wavelength-dependent AMFs before fitting so that the vertical column densities (VCDs) are retrieved directly. The fitting uncertainties of BrO VCDs typically vary between 4 and 7×10^{12} molecules cm^{-2} (~10-20% of the measured BrO VCDs). The retrievals agree well with GOME-2 observations at simultaneous nadir overpasses and ground-based zenith-sky measurements at Harestua, Norway, with mean biases less than $-0.216\pm1.13\times10^{13}$ molecules cm^{-2} and $0.12\pm0.76\times10^{13}$ molecules cm^{-2}, respectively. Global distribution and seasonal variation of OMI BrO are generally consistent with previous satellite observations. Global distribution of BrO from OMBRO shows spatial and temporal patterns similar to GOME-2 retrievals. The OMBRO retrievals show enhancement of BrO over U.S. Great Salt Lake. It also shows significant BrO enhancement from the eruption of the Eyjafjallajökull volcano, although the BrO retrievals are affected under high SO_2 loading conditions by the sub-optimum choice of SO_2 cross sections.

1 Introduction

Bromine monoxide (BrO) is a halogen oxide, predominantly located in the stratosphere and upper troposphere where, like chlorine monoxide (ClO), it is a catalytic element in the destruction of stratospheric ozone (Hausmann and Platt, 1994); von Glasow *et al*., 2004; Salawitch *et al*., 2005; Simpson *et al*., 2007; Abbatt, *et al*., 2012), but with higher efficiency per molecule. Sources of tropospheric BrO include bromine release ("explosions") during the Polar Spring (Hollwedel *et al*., 2004; Begoin *et al*., 2010; Salawitch *et al*., 2010; Blechschmidt *et al*., 2016), volcanic eruption (Bobrowski *et al*., 2003; Chance, 2006; Theys *et al*., 2009;), salt lakes (Hebestreit, *et al*., 1999; Hörmann *et al*. 2016) and stratospheric transport (Salawitch *et al*., 2010). Global BrO measurements from space were first proposed for the Scanning Imaging Absorption Spectrometer for Atmospheric Cartography (SCIAMACHY) instrument (Chance *et al*., 1991) and were first demonstrated with Global Ozone Monitoring Experiment (GOME-1) measurements (Chance, 1998; Platt and Wagner, 1998; Richter *et al*., 1998), and since with SCIAMACHY nadir (Kühl *et al*., 2008) and Global Ozone Monitoring Experiment 2 (GOME-2) measurements (Theys *et al*., 2011). Initial observations of BrO by OMI were first reported by Kurosu *et. al*. (2004). Polar Spring BrO enhancements are known to be associated with boundary layer ozone depletion (Hausmann and Platt, 1994; von Glasow *et al*., 2004; Salawitch *et al*., 2005; Simpson *et al*., 2007; Salawitch *et al*., 2010; Abbatt, *et al*., 2012). OMI measurements of BrO have been used together with chemical and dynamical modeling to investigate stratospheric versus tropospheric enhancements of atmospheric BrO at high northern latitudes (Salawitch *et al*., 2010). OMI BrO retrieval using the Differential Optical Absorption Spectroscopy (DOAS) method has been used to study the seasonal variations of tropospheric bromine monoxide over the Rann of Kutch salt marsh (Hörmann *et al*. 2016). The Arctic Research of the Composition of the Troposphere from Aircraft and Satellites (ARCTAS) campaign (Choi *et al*., 2012) found consistency between BrO column densities calculated from Chemical Ionization Mass Spectrometer (CIMS) measurements with the tropospheric BrO columns derived from OMI using our operational retrieval algorithm. BrO has been observed from the ground in Harestua, Norway (Hendrick *et al*., 2007), Lauder, New Zealand (Schofield *et al*., 2004a, 2004b), Antarctica (Schofield *et al*., 2006), and Barrow, Alaska (Frieß et al., 2011; Liao et al., 2012a,b; Sihler *et al*., 2012; Peterson *et al*., 2016), Eureka, Canada (Zhao *et al*., 2015), Summit, Greenland (Stutz *et al*., 2011) and the Arctic Ocean (Burd *et al*., 2017).

Enhancement of BrO in the vicinity of salt lakes like the Dead Sea and the Great Salt Lake have been observed from ground-based measurements (Hebestreit *et al.*, 1999; Matveev *et al.*, 2001; Stutz *et al.*, 2002; Tas et al., 2005; Holla *et al.*, 2015). The active bromine compound release is due to the reaction between atmospheric oxidants with salt reservoirs. Satellite observation of salt lake BrO was first reported over the Great Salt Lake and the Dead Sea from OMI (Chance, 2006). Seasonal variations of tropospheric BrO over the Rann of Kutch salt marsh have been observed using OMI from an independent research BrO product (Hörmann *et al.* 2016). Bobrowski *et al.* (2003) made the first ground-based observations of BrO and SO_2 abundances in the plume of the Soufrière Hills volcano (Montserrat) by multi-axis DOAS (MAX-DOAS). BrO and SO_2 abundances as functions of the distance from the source were measured by MAX-DOAS in the volcanic plumes of Mt. Etna in Sicily, Italy and Villarica in Chile (Bobrowski *et al.*, 2007). The BrO/SO_2 ratio in the plume of Nyiragongo and Etna was also studied (Bobrowski *et al.*, 2015). The first volcanic BrO measured from space was from the Ambrym volcano, measured by OMI (Chance, 2006). Theys *et al.* (2009) reported on GOME-2 detection of volcanic BrO emission after the Kasatochi eruption. Hörmann *et al.* (2013) examined GOME-2 observations of BrO slant column densities (SCDs) in the vicinity of volcanic plumes; it showed clear enhancements of BrO in ~1/4 of the volcanos, and revealed large spatial differences in BrO/SO2 ratios.

The purpose of this paper is to describe the OMI BrO operational algorithm and the data product, compare it with ground-based and other satellite measurements and analyze its spatiotemporal characteristics. This paper is organized as follows: Section 2 describes the OMI instrument and the data product. Section 3 gives a detailed description of the operational algorithm including algorithm and product history, spectral fitting, AMF calculations, destriping, and fitting uncertainties. Section 4 presents results and discussion including comparison with GOME-2 and ground-based zenith-sky measurements at Harestua, Norway, global distribution, seasonality, enhanced BrO from the U.S. Great Salt Lake and Iceland’s Eyjafjallajökull volcano. Section 5 concludes this study.

2 OMI instrument and OMBRO data product

2.1 OMI instrument

OMI was launched on the NASA Earth Observing System (EOS) Aura satellite into a sun-synchronous orbit on 15 July 2004. It is a push-broom imaging spectrometer that observes solar backscattered radiation in the visible and ultraviolet from 270-500 nm in three channels (UV1: 270-310 nm, UV2: 310-365 nm, visible: 350-500 nm) at spectral resolution of 0.42-0.63 nm and spatial resolution in the normal (global sampling) mode ranging from 13×24 km^2 at direct nadir to about 28×150 km^2 at the swath edges. The global mode (GM) has 60 ground pixels with a total cross-track swath of 2600 km. There are also spatial and spectral zoom modes with twice finer across-track spatial resolution at nadir. The spatial zoom mode (SZM) is employed every 32 days (Levelt *et al.*, 2006): data from this mode are spatially rebinned to global-mode sampling sizes, known as the rebinned spatial zoom mode. The SZM, like the global mode (GM), has 60 cross-track pixels. These are re-binned to 30 pixels, to form “the rebinned spatial zoom mode” (RSZM) which is equivalent in pixel size to the GM data, but with reduced spatial coverage.

Since June 2007, certain cross-track positions of OMI data have been affected by the row anomaly (http://projects.knmi.nl/omi/research/product/rowanomaly-background.php): some loose thermal insulating material likely appeared in front of the instrument’s entrance slit, which can block and scatter the light thus causing errors in level 1b data and subsequently the level 2 retrievals (Kroon *et al.*, 2011). Initially, the row anomaly only affected a few positions and the effect was small. But since January 2009, the anomaly has become more serious, spreading to ~1/3 of the positions and retrievals at those positions are not recommended for scientific use. A flagging field has been introduced in the OMI level 1b data to indicate whether an OMI pixel is affected by this instrument anomaly.

OMI measures ozone and other trace gases, aerosols, clouds, and surface properties. Products developed at the SAO include operational BrO, chlorine dioxide (OClO), and formaldehyde (H_2CO; González Abad *et al.*, 2015) that are archived at NASA Goddard Earth Sciences (GES) Data and Information Services Center (DISC), and offline (“pre-operational”) ozone profile and tropospheric ozone (O_3) (Liu *et al.*, 2010; Huang *et al.*, 2017, 2018), glyoxal ($C_2H_2O_2$) (Chan Miller *et al.*, 2014, 2016) and water vapor (H_2O) (Wang *et al.*, 2014, 2016) that are available at the Aura validation data center (AVDC). All the products except for the ozone profile product are produced using nonlinear least-squares (NLLS) fitting methods based on those previously developed at the SAO for the analysis of measurements from the GOME (now GOME-1) (Chance, 1998; Chance, *et al.*, 2000) and SCIAMACHY instruments (Burrows and Chance, 1991; Chance *et al.*, 1991; Martin *et al.*, 2006).

2.2 OMBRO data product

The current operational BrO product, OMBRO version 3.0.5, contains BrO vertical column densities (VCDs), slant column densities (SCDs), effective air mass factors (AMFs) and ancillary information retrieved from calibrated radiance and irradiance spectra in OMI GM and RSZM level 1b data product. Each BrO product file contains a single orbit of data, from pole to pole, for the sunlit portion of the orbit. The data product from 26 August 2004 through the present is available at GES DISC. Data used in this study cover the period from 1 January 2005 to 31 December 2014.

3 Retrieval algorithm

3.1 Algorithm and product history

OMBRO Version 1.0 was released on 1 February 2007, based on a spectral fitting window of 338–357 nm. Version 2.0 was released on 13 April 2008. It included major adjustments for Collection 3 Level 1b data, improved destriping measures, change of the fitting window to 340–357.5 nm, improvements to radiance wavelength calibration, and several improvements for processing near-real-time data. In both Versions 1 and 2, total BrO VCDs were retrieved in two steps: first performing spectral fitting using the basic optical absorption spectroscopy (BOAS) method to derive SCDs from OMI radiance spectra, and then converting from SCDs to VCDs by dividing AMFs. This is similar to current SAO H_2CO, H_2O and $C_2H_2O_2$ as mentioned previously. The latest Version 3.0.5, released on 28 April 2011, includes major algorithm changes: the fitting window was moved to 319.0–347.5 nm, and BrO cross sections are multiplied by wavelength-dependent AMFs, which are a function of albedo, before fitting, for a direct retrieval of BrO VCDs. SCDs are similarly retrieved in a separate step by fitting BrO cross sections that have not been multiplied with wavelength-dependent AMFs, and an effective AMF = SCD/VCD is computed. Diagnostic cloud information from the OMCLDO2 product (Acarreta *et al.*, 2004) was added, and the row-anomaly indicating flags were carried over from the level 1b product.

The current algorithm is described in detail in the rest of this section, with spectral fitting in Section 3.2, AMF calculation prior to spectral fitting in Section 3.3, post-processing de-stripping to remove cross-track dependent biases in Section 3.4, and fitting uncertainties in Section 3.5.

3.2 Spectral fitting

Most aspects of the algorithm physics for the direct fitting of radiances by the BOAS method were developed previously at SAO for analysis of GOME and SCIAMACHY satellite spectra (Chance, 1998, Chance *et al.*, 2000, OMI, 2002; Martin *et al.*, 2006) and in the various algorithm descriptions of other SAO OMI products (Wang *et al.*, 2014; Chan Miller *et al.*, 2014; Gonzalez Abad *et al.*, 2015). Unlike the often-used DOAS fitting method (Platt, 1994), radiances are not ratioed to irradiances, logarithms are not taken, and no high-pass filtering is applied.

The spectral fitting in the SAO OMI BrO retrieval is based on a Gauss-Newton NLLS fitting procedure, the CERN ELSUNC procedure (Lindström and Wedin, 1987), which provides for bounded NLLS fitting. Processing begins with wavelength calibration for both irradiance and radiance. In each case the wavelength registration for the selected fitting window is determined independently for each cross-track position by cross-correlation of OMI spectra with a high spectral resolution solar irradiance (Caspar and Chance, 1997; Chance, 1998; Chance and Kurucz, 2010) using the preflight instrument slit functions (Dirksen *et al.*, 2006). To improve cross-track stripe correction (Section 3.4) and reduce the noise in the solar irradiance data, the OMI irradiance spectra are composites derived from a principal component analysis of three years of individual OMI irradiance measurements (2005-2007). Radiance wavelength calibration is performed for a representative scan line of radiance measurements (usually in the middle of the orbit) to determine a common wavelength grid for reference spectra.

Following wavelength correction, an undersampling correction spectrum is computed to partially correct for spectral undersampling (lack of Nyquist sampling: Chance, 1998; Slijkhuis *et al.*, 1999; Chance *et al.*, 2005). The calculation of the corrections for the undersampling is accomplished by convolving the preflight slit functions with the high-resolution solar spectrum and differencing its fully-sampled and undersampled representations (Chance *et al.*, 2005).

Fitting is then performed for all scan lines in the OMI swath granule. In each stage, the fitting is performed individually for the 60 cross-track pixels of a block of 100 OMI across-track swath lines along the flight direction (30 cross-track pixels for the RSZM) according to Eq. (1):

$$I = \left\{(aI_0 + \textstyle\sum_i \alpha_i A_i)e^{-\sum_j \beta_j B_j} + \sum_k \gamma_k C_k\right\} Poly_{scale} + Poly_{baseline}\ , \qquad (1)$$

where I_0 is the solar irradiance (used in our operational BrO retrieval) or radiance reference measurement, I is the Earthshine radiance (detected at satellite), a is albedo, α_i, β_j, γ_k, are the coefficients to the reference spectra of A_i, B_j, C_k, (for example, trace gas cross sections, Ring effect, vibrational Raman, undersampling correction, common mode, *etc.*) of model constituents. The reference spectra are derived separately for each cross-track position from original high-resolution cross sections convolved with the corresponding OMI slit functions after correcting for the solar I_0 effect (Aliwell *et al.*, 2002). Fig. 1 shows the trace gas cross sections and Ring spectra used in the current operational algorithm. The black lines are the original high-resolution reference spectra, and the color lines show the corresponding spectra convolved with OMI slit function, which are used in the fitting.

For improved numerical stability, radiances and irradiances are divided by their respective averages over the fitting window, renormalizing them to values of ~1. BrO is fitted in the spectral window 319.0–347.5 nm, within the UV-2 channel of the OMI instrument. The switch from the previous fitting window of 340–357.5 nm to this shorter and wider fitting window is to reduce fitting uncertainty by including more BrO spectral structures as shown in Fig. 1.

The rotational Raman scattering (Chance and Spurr, 1997; Chance and Kurucz, 2010) and undersampling correction spectra, A_i, are first added to the albedo-adjusted solar irradiance aI_0, with coefficients α_i as shown in Eq. 1. Radiances I are then modeled as the this quantity attenuated by absorption from BrO, O_3, NO_2, H_2CO, and SO_2 with coefficients β_j fitted to the reference spectra B_j as shown in Eq. 1. A common mode spectrum C_k, computed on line, is added by fitting coefficient γ_k after the Beer-Lambert law contribution terms. An initial fit of several hundred pixels per cross-track position determines the common mode spectra (one spectrum per cross-track position, between 30°N and 30°S) as the average of the fitting residuals. The common mode spectra include any instrument effects that are uncorrelated to molecular scattering and absorption. This is done to reduce the fitting root-mean-square (RMS) residuals, and the overall uncertainties. These are then applied as reference spectra in fitting of the entire orbit. The fitting additionally contains additive ($Poly_{baseline}$) and multiplicative closure polynomials ($Poly_{scale}$), parameters for spectral shift and, potentially, squeeze (not normally used). The operational parameters and the cross sections used are provided in Table 1.

3.3 Air mass factors

Due to significant variation in ozone absorption and Rayleigh scattering in the fitting window AMFs vary with wavelength by 10-15% as shown in Fig. 2. At large solar and viewing zenith angles it is difficult to identify a single representative AMF *ad hoc*. The wavelength dependent AMFs are introduced to take into account for such strong variation within the BrO fitting window. They are applied pre-fit to the BrO cross sections, and the spectral fit retrieves VCDs directly. This direct fitting approach is a major departure from the commonly employed 2-step fitting procedure (OMI, 2002). It was first developed for retrievals of trace gases from SCIMACHY radiances in the shortwave infrared (Buchwitz *et al*., 2000) and has been demonstrated for total O_3 and SO_2 retrievals from GOME/SCIAMACHY measurements in the ultraviolet (Bracher *et al.*, 2005; Coldewey-Egbers *et al.*, 2005; Weber et al., 2005; Lee *et al.*, 2008).

The albedo- and wavelength-dependent AMFs were pre-computed with the Linearized Discrete Ordinate Radiative Transfer code (LIDORT, Spurr, 2006) using a single mostly stratospheric BrO profile (Fig. 3). The BrO profile, based on the model of Yung *et al.* (1980), has ~30% BrO below 15 km, ~10% BrO below 10 km, and ~2% BrO below 5 km. For conditions with enhanced BrO in the lower troposphere, using this profile will overestimate the AMFs and therefore underestimate the BrO VCDs. Surface albedos are based on a geographically varying monthly mean climatology derived from OMI (Kleipool *et al.,* 2008). Although AMFs based on this BrO profile only slightly depend on surface albedo, albedo effects can be significant over highly reflective snow/ice surfaces, reducing VCDs by 5-10%.

In order to provide the AMF in the data product for consistency with previous versions based on a two-step approach, a second fitting of all OMI spectra is performed with unmodified BrO cross sections, which yields SCDs. An effective AMF can then be computed as AMF = SCD/VCD.

The salmon color line in bottom panel of Fig. 1 shows the modified BrO cross section after multiplication with the wavelength-dependent AMF (albedo = 0.05, SZA = 5.0°, and VZA = 2.5°). The wavelength-dependence in AMF is visible from the varying differences near BrO absorption peaks and the right wings at different wavelengths. The correlation of the unmodified BrO cross sections with the rest of the fitted molecules is small (typically less than 0.12), except with H_2CO (0.43). However, it is safe to assume that in most polar regions with enhanced BrO there are no high concentrations of formaldehyde. It will be worthwhile for future studies to assess the interference of H_2CO under high H_2CO and background BrO conditions. In addition, the AMF wavelength dependence increases with the increase of solar and viewing zenith angles and surface albedo, which increases the correlation between modified BrO cross sections and O_3 cross sections. However, the correlation with O_3 becomes noticeable (~0.10) only at solar zenith angles above ~80°.

3.4 Destriping

OMI L1b data exhibit small differences with cross-track position, due to differences in the dead/bad pixel masks (cross-track positions are mapped to physically separate areas on the CCD), dark current correction, and radiometric calibration, which lead to cross-track stripes in Level 2 product (Veihelmann and Kleipool, 2006). Our destriping algorithm employs several methods to reduce cross-track striping of the BrO columns. First, we screen outliers in the fitting residuals. This method, originally developed to mitigate the effect of the South Atlantic Anomaly in SAO OMI BrO, H_2CO, and OClO data products, is now also being employed for GOME-2 (Richter *et al.*, 2011). Screening outliers is done through computing the median, r_{med}, and the standard deviation σ of residual spectra $r(\lambda)$ and in subsequent refitting excluding any spectral points for which $r(\lambda) \geq |r_{med} \pm 3\sigma|$. This can be done repeatedly for every ground pixel, which makes the processing slow. However, we do it once for a reference scan line, recording the positions of the bad pixels, and excluding them by default in each subsequent fit. Second, after the completion of the spectral fitting process for all ground pixels in the granule, a post-processing cross-track bias correction is performed: an average cross-track pattern is calculated from the along-track averages of all BrO VCDs for each cross-track position within a ±30° latitude band around the equator, to which a low-order polynomial is fitted. The differences between the cross-track pattern and the fitted polynomial is then applied as a cross-track VCD correction (or “smoothing”) factor. The smoothed VCDs are provided in a separate data field, *ColumnAmountDestriped*. Smoothed SCDs are derived in an analogous fashion and are also included in the data product.

3.5 Fitting uncertainties

Estimated fitting uncertainties are given as $\sigma_i = \sqrt{C_{ii}}$ where C is the covariance matrix of the standard errors. This definition is strictly true only when the errors are normally distributed. In the case where the level 1 data product uncertainties are not reliable estimates of the actual uncertainties, spectral data are given unity weight over the fitting window, and the 1σ fitting error in parameter i is determined as

$$\sigma_i = \varepsilon_{rms}\sqrt{\frac{c_{ii} \times npoints}{npoints - nvaried}} \qquad (2)$$

where ε_{rms} is the root mean square of the fitting residuals, *npoints* is the number of points in the fitting window, and *nvaried* is the number of parameters varied during the fitting.

The BrO VCD retrieval uncertainties listed in the data product only include spectral fitting errors. Error sources from AMFs (*i.e.*, BrO climatology), atmospheric composition and state (pressure/temperature vertical profiles, total ozone column, *etc.*) and other sources of VCD uncertainty are not included. The fitting uncertainties for single measurements of the BrO VCDs typically vary between 4×10^{12} and 7×10^{12} molecules cm^{-2}, consistently throughout the data record. The uncertainties vary with cross-track positions, from ~7×10^{12} at nadir positions to ~4×10^{12} at edge positions due to the increase of photon path length through the stratosphere. Relatively, the VCD uncertainties typically range between 10-20% of individual BrO VCDs, but could be as low as 5% over BrO hotspots. This is roughly 2-3 times worse that what was achieved from GOME-1 data. Uncertainties in the AMF, used to convert slant to vertical columns, are estimated to be 10%

or less except when there is substantially enhanced tropospheric BrO. Hence the total uncertainties of the BrO vertical columns typically range within 15-30%.

4 Results and discussions

Comparisons of the OMI OMBRO product with GOME-2 satellite retrievals and remote sensing ground based measurements over Harestua, Norway as well as monthly mean averages illustrate the quality of the retrieval on a global scale. On a local scale, recent scientific studies looking at BrO enhancements in volcanic plumes and over salt lakes are pushing the limits of the current OMBRO setups. In the following sections, we provide details of these comparisons (section 4.1) and discuss OMI OMBRO global distribution (section 4.2) and local enhancements over salt lakes and volcanic plumes observations (section 4.3), and their applicability and strategies to correctly use the publicly available OMBRO product.

4.1 Comparisons with GOME-2 and ground-based observations

To assess the quality of the OMBRO product, we first compared OMI BrO VCDs with BIRA/GOME-2 BrO observations (Theys *et al.*, 2011). GOME-2 and OMI have different orbits: descending orbit with a local equator crossing time (ECT) of 9:30 am for GOME-2 and afternoon ascending orbit with an ECT of 1:45 pm for OMI. To minimize the effects of diurnal variation especially under high solar zenith angles (e.g., McLinden *et al.*, 2006; Sioris *et al.*, 2006) on the comparison, we conduct the comparison using simultaneous nadir overpasses (SNOs) within 2 minutes between GOME-2 and OMI predicted by NOAA National Calibration Center's SNO prediction tool （https://ncc.nesdis.noaa.gov/SNOPredictions）. Due to different orbits, all these SNOs occur at high latitudes around 75°S/N. Fig. 4 shows the time series of comparison of individual OMI/GOME-2 BrO from February 2007 through November 2008. The temporal variation of BrO at the SNO locations is captured similarly by OMI and GOME-2 BrO. The scatter plot in Fig. 5 quantifies the comparison between OMI and GOME-2 BrO. OMI BrO shows excellent agreement with GOME-2 BrO with a correlation of 0.74, and a mean bias of -0.216 ± 1.13×10^{13} molecules cm^{-2} (mean relative bias of -2.6 ± 22.1%). Considering very different retrieval algorithms including different cross sections and BrO profiles, such a good agreement is remarkable. GOME-2 retrievals use the BrO cross sections of Fleischmann *et al.* (2004) while our BrO retrievals use the BrO cross sections of Wilmouth *et al.* (1999). According to the sensitivity studies by Hendrick *et al.* (2009), using the Fleischmann cross section increases BrO by ~10%. So, accounting for different cross sections, OMI BrO underestimates the GOME-2 BrO by ~10%. In addition, the GOME-2 algorithm uses a residual technique to estimate tropospheric BrO from measured BrO SCDs by subtracting a dynamic estimate of stratospheric BrO climatology driven by O_3 and NO_2 concentrations and by using two different tropospheric BrO profiles depending on surface albedo conditions. This is very different from the approach of using a single BrO profile in the OMI BrO algorithm, and can contribute to some of the BrO differences. Furthermore, additional algorithm uncertainties in both algorithms and different spatial sampling can also cause some differences.

We also used ground-based zenith-sky measurements of total column BrO at Harestua, Norway (Hendrick *et al.*, 2007) to estimate the quality of the OMI BrO. We compared daily mean total BrO at Harestua with the mean OMI BrO from individual footprints that contain the location of Harestua site. Fig. 6 shows the time series of the comparison between OMI total BrO and Harestua total BrO from February 2005 through August 2011 with the scatter plot shown in Fig. 7. Ground-based BrO shows an obvious seasonality with high values in the winter/spring and low values in the summer/fall. Such seasonality is well captured by OMI BrO. OMI BrO shows a reasonable good agreement with Harestua BrO with a correlation of 0.46 and a mean bias of $0.12\pm0.76\times10^{13}$ molecules cm^{-2} (mean relative bias of 3.18±16.30%, with respect to individual Harestua BrO). Sihler *et al.* (2012) compared GOME-2 BrO to ground-based observations at Barrow finding the correlation to be weaker (r = 0.3), likely due to both elevated and shallow surface layers of BrO. However, their correlation between GOME-2 BrO and ground-based measurements at Amundsen, U.S. (r = 0.4) is closer to our correlation here. From the Harestua data, tropospheric BrO typically consists of 15-30% of the total BrO, larger than what we have assumed in the troposphere. The use of a single BrO profile in the OMI BrO algorithm will likely underestimate the actual BrO. Accounting for the uncertainty due to profile shape, OMI BrO will have a larger positive bias relative to Harestua measurements, which can be caused by other algorithm uncertainties and the spatiotemporal differences between OMI and Harestua BrO.

4.2 Global distribution of BrO VCDs

Fig. 8 presents the global distribution of monthly mean BrO VCDs for selected months (March, June, September, December) showing BrO seasonality for three different years (2006, 2007 and 2012). BrO typically increases with latitude, with minimal values in the tropics (~2×10^{13} molecules cm^{-2}) and maximum values (~10^{14} molecules cm^{-2}) around polar regions especially in the northern hemisphere winter/spring. In the tropics, BrO shows little seasonality but at higher latitudes in polar regions, BrO displays evident seasonality. The seasonality is different between northern and southern hemispheres. In the northern hemisphere, BrO values are larger in the winter/spring and smaller in the summer/fall, and the enhancement is more widespread during the spring. In the southern hemisphere, BrO values are larger in southern hemispheric spring and summer (i.e., September and January) and smaller in the winter. Such global distribution and seasonal variation are generally consistent with previous satellite measurements (*cf.* Chance, 1998; http://bro.aeronomie.be/level3_monthly.php?cmd=map). BrO in the tropics shows consistent zonal distributions with lower values over land and in the intertropical convergence zone. This might be related to the impacts of clouds on the retrievals (e.g, BrO below thick clouds cannot be measured, there are uncertainties in the AMF calculation under cloudy conditions) and will be investigated in detail in future studies. The global distribution and seasonal variation are consistent from year to year, but the distributions from different years disclose some interannual variation. For example, BrO values in 2007 are smaller in January but are larger in March compared to those in 2006. Although OMI data since 2009 have been seriously affected by the row anomaly at certain cross-track positions, the monthly mean data derived from good cross-track positions are hardly affected by the row anomaly as shown from the very similar global distribution and seasonality in 2012.

4.3 Salt lakes and volcanic plumes enhancements of BrO

Following recent work by Hörmann et al. (2016) we have checked the capability of OMBRO to observe similar enhancements in other salt lakes. Fig. 9 shows monthly averaged OMI BrO over the Great Salt Lake for 02/2013. And the Dead Sea for 07/2009. Over the Great Salt Lake, BrO enhancement occurs predominantly over the lake bed with enhancements of ~$5\text{-}10\times10^{12}$ molecules cm^{-2} over background values ($4\text{-}4.7\times10^{13}$ molecules cm^{-2}). Over the Dead Sea, the BrO enhancement of $5\text{-}8\times10^{12}$ molecules cm^{-12} occurs to the South-West, where BrO accumulates at a small hill due to the prevailing north-easterly winds. Despite observing these enhancements, the users of OMBRO for these kinds of studies should be aware of two limitations of the current retrieval. First, the actual BrO enhancement is actually underestimated since we are assuming a mostly stratospheric BrO profile for the AMF. Second, the OMI derived albedo climatology (Kleipool et al. 2008) used in OMBRO has a resolution of 0.5 degrees. At this resolution OMBRO retrievals can have biases given the size of OMI pixels and sub-pixel albedo variability not represented in the albedo climatology. We also raise attention to the fact that abnormally high cloud fractions are reported over the salt lakes due to enhanced albedos. All these considerations are important for future studies studying spatiotemporal distribution of BrO over salt lakes.

During our analysis of volcanic eruption scenarios, it was discovered that the currently implemented SO_2 molecular absorption cross sections (Vandaele *et al.*, 1994) are a sub-optimum choice (see Fig. 10). Compared to more recent laboratory measurements (Hermans *et al.*, 2009; Vandaele *et al.*, 2009), the original SO_2 cross sections implemented in OMBRO do not extend over the full BrO fitting window and exhibit the wrong behavior longward of 324 nm, overestimating the most recent measurement by up to a factor of 3. As the correlation between BrO and both SO_2 cross sections are very small (-0.03 for the current SO_2 and 0.11 for the latest SO_2 cross sections) over the spectral range of SO_2 cross sections, interference by SO_2 in BrO retrievals is usually not an issue at average atmospheric SO_2 concentrations, but strong volcanic eruptions will render even small SO_2 absorption features past 333 nm significant. Around 334 nm, the Vandaele *et al.* (2009) data show an SO_2 feature that correlates with BrO absorption when SO_2 concentrations are significantly enhanced. As a consequence of this spectral correlation, SO_2 may be partially aliased as BrO, since the implemented SO_2 cross sections cannot account for it. Fig. 11 presents an example from the 2010 Eyjafjallajökull eruption to show that the BrO retrieval can be affected by the choice of SO_2 cross sections. The next version of the OMBRO public release will be produced using the updated SO_2 absorption cross sections. Until then, caution is advised when using the OMI BrO product during elevated SO_2 conditions. We recommend to use OMBRO product together with the operational OMI SO_2 product (Li *et al.*, 2013) to flag abnormally high BrO retrievals.

The top panels of Fig. 11 show daily average operational BrO VCDs from the eruption of the Eyjafjallajökull volcano on May 5 and 17, 2010, respectively. Enhanced BrO values in excess of 8.0×10^{13} are detected in the vicinity of this volcano (e.g., plume extending southeast ward from the volcano on May 5 and, high BrO over Iceland on May 17). Some of these enhanced BrO values correspond to the locations of enhanced SO_2 as shown from the NASA global SO_2 monitoring website (https://so2.gsfc.nasa.gov/). This enhancement of BrO is not related to the seasonal variation of BrO as no such BrO enhancement is detected over Eyjafjallajökull during May 5-17, 2011 (a year after the eruption), with BrO values of only up to $\sim5.3\times10^{13}$ molecules cm^{-2} (not shown). The bottom panels of Fig. 11 show the same BrO retrievals using SO_2 cross sections by Vandaele et al. (2009). Using the improved SO_2 cross sections increase the BrO over a broader area on both days, supporting that the choice of SO_2 cross sections can affect the BrO retrievals. However, BrO enhancement around the volcano can still clearly be seen with the improved SO_2 cross sections. This suggests that this BrO enhancement is not totally due to aliasing of SO_2 as BrO, but real BrO from the volcanic eruption.

5 Conclusions

This paper describes the current operational OMI BrO retrieval algorithm developed at SAO and the corresponding V3.05 OMI total BrO (OMBRO) product in detail. The OMI BrO retrieval algorithm is based on nonlinear least-squares direct fitting of radiance spectra in the spectral range 319.0-347.5 nm to obtain vertical column densities (VCDs) directly in one step. Compared to previous versions of two-step algorithms, the fitting window was moved to shorter wavelengths and the spectral range was increased to reduce the fitting uncertainty. Because air mass factors (AMFs) vary significantly with wavelengths as a result of significant variation of ozone absorption, the wavelength and surface albedo dependent AMF, which is precomputed with the Linearized Discrete Ordinate Radiative Transfer (LIDORT) code using a single mostly stratospheric BrO profile, is applied pre-fit to BrO cross sections for direct fitting of VCDs. Prior to the spectral fitting of BrO, wavelength calibration is performed for both irradiance and radiance at each cross-track position and reference spectra are properly prepared at the radiance wavelength grid. Then radiances are modeled from the measured solar irradiance, accounting for rotational Raman scattering, undersampling, attenuation from BrO and interfering gases, and including additive and multiplicative closure polynomials, and the average fitting residual spectrum. To maintain consistency with previous versions, a second fitting of all OMI spectra is performed with unmodified BrO cross sections to derive SCDs and the effective AMFs. Then a destriping step is employed to reduce the cross-track dependent stripes.

The uncertainties of BrO VCDs included in the data product include only spectral fitting uncertainties, which typically vary between 4 and 7×10^{12} molecules cm^{-2} (10-20% of BrO VCDs, could be as low as 5% over BrO hotspots), consistent throughout the data record. The uncertainties vary with cross-track positions, from ~7×10^{12} at nadir positions to ~4×10^{12} at edge positions. The use of single stratospheric BrO profile is another source of uncertainty, overestimating AMFs and therefore underestimating BrO VCDs for conditions with enhanced BrO in the lower troposphere. In addition, the used SO_2 cross sections are a sub-optimum choice and can cause errors in the retrievals under high SO_2 concentrations.

We compared OMI BrO VCDs with BIRA/GOME-2 BrO observations at locations of simultaneous nadir overpasses. OMI BrO shows excellent agreement with GOME-2 BrO with a correlation of 0.74, and a mean bias of -0.216±1.13x10^{13} molecules cm^{-2} (mean relative bias of -2.6 ± 22.1%). We also compared OMI BrO with ground-based zenith-sky measurements of total BrO at Harestua, Norway. This BrO seasonality in Harestua total BrO is well captured by the OMI BrO and OMI BrO shows a reasonable good agreement with a moderate correlation of 0.46 and a small mean bias of 0.12±0.76×10^{13} molecules cm^{-2} (mean relative bias of 3.18±16.30%). The global distribution and seasonal variation of OMI BrO are generally consistent with previous satellite measurements. There are small values in the tropics with no much seasonality, and large values at high latitudes with distinct seasonality. And the seasonality is different between the northern and southern hemisphere, with larger values in the hemispheric winter/spring (spring/summer) and smaller values in summer/fall (winter) for the northern (southern) hemisphere. This spatiotemporal variation is generally consistent from year to year and is hardly affected by the row anomaly, but does show some interannual variation. The retrievals show enhanced BrO of 5-10×10^{12} molecules cm^{-2} over the U.S. Great Salt Lake and the Dead Sea Valley, and also significant enhancement from the eruption of Eyjafjallajökull volcano despite BrO retrievals under high SO_2 conditions can be affected by the current use of a sub-optimal choice of SO_2 cross sections.

For the next version, we will update the SO_2 cross sections, test the inclusion of O_2-O_2 cross sections, optimize the spectral fitting including investigating and mitigating the interference of H_2CO on BrO retrieval. We will also improve the AMF calculation accounting for clouds and ozone and consider the use of model-based climatological BrO profiles. The second step of spectral fitting to derive SCDs and effective AMFs will be removed as the effective AMFs can be derived from wavelength dependent AMFs.

Acknowledgements

This study is supported by NASA Atmospheric Composition Program/Aura Science Team (NNX11AE58G) and the Smithsonian Institution. Part of the research was carried out at the Jet Propulsion Laboratory, California Institute of Technology, under a contract with NASA. The Dutch-Finnish OMI instrument is part of the NASA EOS Aura satellite payload. The OMI project is managed by NIVR and KNMI in the Netherlands. We acknowledge the OMI International Science Team for providing the SAO OMBRO data product used in this study.

References

Abbatt, J. P. D., Thomas, J. L., Abrahamsson, K., Boxe, C., Granfors, A., Jones, A. E., King, M. D., Saiz-Lopez, A., Shepson, P. B., Sodeau, J., Toohey, D. W., Toubin, C., von Glasow, R., Wren, S. N., Yang, X.: Halogen activation via interactions with environmental ice and snow, Atmos. Chem. Phys., 12, 6237–6271, https://doi.org/10.5194/acp-12-6237-2012, 2012.

Acarreta, J.R., De Haan, J.F., and Stammes, P.: Cloud pressure retrieval using the O_2-O_2 absorption band at 477 nm, J. Geophys. Res-Atmos., 109, http://dx.doi.org/10.1029/2003JD003915, 2004.

Aliwell, S.R., Van Roozendael, M., Johnston, P.V., Richter, A., Wagner, T., Arlander, D.W., Burrows, J.P., Fish, D.J., Jones, R.L., Tornkvist, K.K., Lambert, J.-C., Pfeilsticker, K., Pundt, I., Analysis for BrO in zenith-sky spectra: An intercomparison exercise for analysis improvement, J. Geophys. Res., 107(D14), doi:10.1029/2001JD000329, 2002.

Blechschmidt, A.-M., Richter, A., Burrows, J. P., Kaleschke, L., Strong, K., Theys, N., Weber, M., Zhao, X., Zien, A.: An exemplary case of a bromine explosion event linked to cyclone development in the Arctic, Atmos. Chem. Phys., 16, 1773-1788, https://doi.org/10.5194/acp-16-1773-2016, 2016.

Bobrowski, N., Hönninger, G., Galle, B. and Platt, U.: Detection of bromine monoxide in a volcanic plume, Nature, 423, 273-276, 2003.

Bobrowski, N., von Glasow, R., Aiuppa, A., Inguaggiato, S., Louban, I., Ibrahim, O.W., and Platt, U.: Reactive halogen chemistry in volcanic plumes, J. Geophys. Res. Atmos., 112, D06311, doi:10.1029/2006JD007206, 2007.

Bobrowski, N., von Glasow, R., Giuffrida, G.B., Tedesco, D., Aiuppa, A., Yalire, M., Arellano, S., Johansson, M., and Galle, B.: Gas emission strength and evolution of the molar ratio of BrO/SO_2 in the plume of Nyiragongo in comparison to Etna, J. Geophys. Res Atmos., 120, 277-291, doi:10.1002/2013JD0 21069, 2015.

Bracher, A., Lamsal, L.N., Weber, M., Bramstedt, K., Coldewey-Egbers, M., and Burrows, J.P.: Global satellite validation of SCIAMACHY O3 columns with GOME WFDOAS, Atmos. Chem. Phys., 5, 2357-2368, https://doi.org/10.5194/acp-5-2357-2005, 2005.

Buchwitz, M., Rozanov, V.V., and Burrows, J.P.: A near-infrared optimized DOAS method for the fast global retrieval of atmospheric CH_4, CO, CO_2, H_2O, and N_2O total column amounts from SCIAMACHY Envisat-1 nadir radiances, J. Geophys. Res., D105, 15231–15245, 2000.

Burd, Justine A., Peterson, Peter K., Nghiem, Son V., Perovich, Don K., Simpson, William R.: Snowmelt onset hinders bromine monoxide heterogeneous recycling in the Arctic, J. Geophys. Res, Atmos., 122, 8297-8309, 2017.

Burrows, J.P. and Chance, K.V.: Scanning Imaging Absorption Spectrometer for Atmospheric ChartographY, Proc. S.P.I.E., Future European and Japanese Remote Sensing Sensors and Programs, 1490 146-154, 1991.

Caspar, C. and Chance, K.: GOME wavelength calibration using solar and atmospheric spectra, in: Third ERS Symposium on Space at the service of our Environment, edited by: Guyenne, T.-D. and Danesy, D., Vol. 414 of ESA Special Publication, p. 609, 1997.

Chan Miller, C., González Abad, G., Wang, H., Liu, X., Kurosu, T., Jacob, D.J., and Chance, K.: Glyoxal retrieval from the Ozone Monitoring Instrument, Atmos. Meas. Tech., 7, 3891-3907, 2014.

Chan Miller, C., Jacob, D.J., González Abad, G., and Chance, K.: Hotspot of glyoxal over the Pearl River Delta seen from the OMI satellite instrument: Implications for emissions of aromatic hydrocarbons, Atmos. Chem. Phys., 16, 4631-4639, doi:10.5194/acp-16-4631-2016, 2016.

Chance, K. and Kurucz, R., An improved high-resolution solar reference spectrum for earth's atmosphere measurements in the ultraviolet, visible, and near infrared, J. Quant. Spectrosc. Radiat. Transfer, 111, 1289–1295, doi:10.1016/j.jqsrt.2010.01.036, 2010.

Chance, K., and Orphal, J.: Revised ultraviolet absorption cross sections of H_2CO for the HITRAN database, J. Quant. Spectrosc. Radiat. Transfer, 112, 1509-1510, doi:10.1016/j.jqsrt.2011.02.002, 2011.

Chance, K., and Kurucz, R.L.: An improved high-resolution solar reference spectrum for Earth's atmosphere measurements in the ultraviolet, visible, and near infrared, J. Quant. Spectrosc. Radiat. Transfer, 111, 1289-1295, 2010.

Chance, K., Kurosu, T.P., and Sioris, C.E.: Undersampling correction for array-detector based satellite spectrometers, Appl. Opt., 44, 1296-1304, 2005.

Chance, K., Palmer, P.I., Spurr, R.J.D., Martin, R.V., Kurosu, T.P., and Jacob, D. J.: Satellite observations of formaldehyde over North America from GOME, Geophys. Res. Lett., 27, 3461–3464, doi:10.1029/2000GL011857, 2000.

Chance, K.: Analysis of BrO measurements from the Global Ozone Monitoring Experiment, Geophys. Res. Lett., 25, 3335-3338, 1998.

Chance, K.: Spectroscopic Measurements of Tropospheric Composition from Satellite Measurements in the Ultraviolet and Visible: Steps Toward Continuous Pollution Monitoring from Space, in “Remote Sensing of the Atmosphere for Environmental Security,” Eds. A. Perrin, N. Ben Sari-Zizi, and J. Demaison, NATO Security through Science Series, ISBN: 1-4020-5089-5, Springer, pp. 1-25, 2006.

Chance, K.V. and Spurr, R.J.D.: Ring effect studies: Rayleigh scattering, including molecular parameters for rotational Raman scattering, and the Fraunhofer spectrum, Appl. Opt., 36, 5224-5230, doi:10.1364/AO.36.005224, 1997.

Chance, K.V., Burrows, J.P., and Schneider, W.: Retrieval and molecule sensitivity studies for the Global Ozone Monitoring Experiment and the SCanning Imaging Absorption spectroMeter for Atmospheric CHartographY, Proc. S.P.I.E., Remote Sensing of Atmospheric Chemistry, 1491, 151-165, 1991.

Choi, S., Wang, Y., Salawitch, R.J., Canty, T., Joiner, J., Zeng, T., Kurosu, T.P., Chance, K., Richter, A., Huey, L.G., Liao, J., Neuman, J.A., Nowak, J.B., Dibb, J.E., Weinheimer, A.J., Diskin, G., Ryerson, T.B., da Silva, A., and Curry, J.: Analysis of satellite-derived Arctic tropospheric BrO columns in conjunction with aircraft measurements during ARCTAS and ARCPAC, Atmos. Chem. Phys., 12, 1255-1285, doi: 10.5194/acp-12-1255-2012, 2012.

Coldewey-Egbers, M., Weber, M., Lamsal, L.N., de Beek, R., Buchwitz, M., and Burrows, J.P.: Total ozone retrieval from GOME UV spectral data using the weighting function DOAS approach, Atmos. Chem. Phys., 5, 1015-1025, https://doi.org/10.5194/acp-5-1015-2005, 2005.

Dirksen, R., Dobber, M., Voors, R., and Levelt, P.: Prelaunch characterization of the Ozone Monitoring Instrument transfer function in the spectral domain, Appl. Opt., 45, 3972-3981, 2006.

Fleischmann, O.C., Hartmann, M., Burrows, J.P., and Orphal, J.: New ultraviolet absorption cross sections of BrO at atmospheric temperatures measured by time-windowing Fourier transform spectroscopy, J. Photochem. Photobiol. A., 168, 117–132, doi:10.1016/j.jphotochem.2004.03.026, 2004.

González Abad, G., Liu, X., Chance, K., Wang, H., Kurosu, T.P., and Suleiman, R.: Updated Smithsonian Astrophysical Observatory Ozone Monitoring Instrument (SAO OMI) formaldehyde retrieval, Atmos. Meas. Tech., 8, 19-32, doi:10.5194/amt-8-19-2015, 2015.

Frieß, U., Sihler, H., Sander, R., PöHler, D., Yilmaz, S., Platt, U.: The vertical distribution of BrO and aerosols in the Arctic: Measurements by active and passive differential optical absorption spectroscopy, J. Geophys. Res., 116, D00R04, doi: 10.1029/2011JD015938, 2011.

Hausmann, M., Platt, U.: Spectroscopic measurement of bromine oxide and ozone in the high Arctic during Polar Sunrise Experiment 1992, J. Geophys. Res., D12, 25399-25413,1994.

Hebestreit, K., Stutz, J., Rosen, D., Matveiv, V., Peleg, M., Luria, M., Platt, U.: DOAS Measurements of Tropospheric Bromine Oxide in Mid-Latitudes, Science, 283, 5398, 55, doi: 10.1126/science.283.5398.55, 1999.

Hendrick, F., Van Roozendael, M., Chipperfield, M.P., Dorf, M., Goutail, F., Yang, X., Fayt, C., Hermans, C., Pfeilsticker, K., Pommereau, J.-P., Pyle, J.A., Theys, N., and De Maziére, M. Retrieval of stratospheric and tropospheric BrO profiles and columns using ground-based zenith-sky DOAS observations at Harestua, 60° N, Atmos. Chem. Phys., 7, 4869-4885, https://doi.org/10.5194/acp-7-4869-2007, 2007.

Hendrick, F., Johnston, P.V., De Mazière, M., Fayt, C., Hermans, C., Kreher, K., Theys, N., Thomas, A., and Van Roozendael, M.: One-decade trend analysis of stratospheric BrO over Harestua (60° N) and Lauder (45° S) reveals a decline, Geophys. Res. Lett., 35, L14801, doi:10.1029/2008gl034154, 2008.

Hendrick, F., Rozanov, A., Johnston, P.V., Bovensmann, H., De Mazière, M., Fayt, C., Hermans, C., Kreher, K., Lotz, W., Sinnhuber, B.-M., Theys, N., Thomas, A., Burrows, J.P., and Van Roozendael, M.: Multi-year comparison of stratospheric BrO vertical profiles retrieved from SCIAMACHY limb and ground-based UV-visible measurements, Atmos. Meas. Tech., 2, 273-285, https://doi.org/10.5194/amt-2-273-2009, 2009.

Hermans, C., Vandaele, A.C., and Fally, S.: Fourier transform measurements of SO_2 absorption cross sections: I. Temperature dependence in the 24 000 - 29 000 cm-1 (345-420 nm) region, J. Quant. Spectrosc. Radiat. Transfer, 110, 756-765, 2009.

Hermans, C., Vandaele, A.C., Fally, S., Carleer, M., Colin, R., Coquart, B., Jenouvrier, A., and Merienne, M.-F.: Absorption cross sections of the collision-induced bands of oxygen from the UV to the NIR, NATO Advanced Research Workshop on Weakly Interacting Molecular Pairs: Unconventional Absorbers of Radiation in the Atmosphere, Eds. C. Camy-Peyret and A. Vigasin, Kluwer Academic Publ., NATO Meeting series, ISBN: 1-4020-1596-8, 193-202, 2003.

Holla, R., Schmitt, S., Frieß, U., Pöhler, D., Zingler, J., Corsmeier, U., Platt, U.: Vertical distribution of BrO in the boundary layer at the Dead Sea, Environ. Chem., 10.1071/EN14224, 12, 4, 438-460, 2015.

Hollwedel, J., Wenig, M., Beirle, S., Kraus, S., Kühl, S., Wilms-Grabe, W., Platt, U., and Wagner, T.: Year-to-year variations of spring time polar tropospheric BrO as seen by GOME, Adv. Space Res., 34, 4, 804-808, 2004.

Hörmann, C., Sihler, H., Bobrowski, N., Beirle, S., Penning de Vries, M., Platt, U., Wagner, T.: Systematic investigation of bromine monoxide in volcanic plumes from space by using the GOME-2 instrument, Atmos. Chem. Phys., 13, 4749-4781, https://doi.org/10.5194/acp-13-4749-2013, 2013.

Hörmann, C., Sihler, H., Beirle, S., Penning de Vries, M., Platt, U., and Wagner, T.: Seasonal variation of tropospheric bromine monoxide over the Rann of Kutch salt marsh seen from space, Atmos. Chem. Phys., 16, 13015-13034, doi:10.5194/acp-16-13015-2016, 2016.

Huang, G., Liu, X., Chance, K., Yang, K., Bhartia, P. K.,Cai, Z., Allaart, M., Ancellet, G., Calpini, B., Coetzee, G.J.R., Cuevas-Agulló, E., Cupeiro, M., De Backer, H., Dubey, M.K., Fuelberg, H.E., Fujiwara, M., Godin-Beekmann, S., Hall, T.J., Johnson, B., Joseph, E., Kivi, R., Kois, B., Komala, N., König-Langlo, G., Laneve, G., Leblanc, T., Marchand, M., Minschwaner, K.R., Morris, G., Newchurch, M.J., Ogino, S.-Y., Ohkawara, N., Piters, A.J.M., Posny, F., Querel, R., Scheele, R., Schmidlin, F.J., Schnell, R.C., Schrems, O., Selkirk, H., Shiotani, M., Skrivánková, P., Stübi, R., Taha, G., Tarasick, D.W., Thompson, A. M.,Thouret, V., Tully, M. B., Van Malderen, R., Vömel, H., von der Gathen, P., Witte, J.C., and Yela, M.: Validation of 10-year SAO OMI Ozone Profile (PROFOZ) product using ozonesonde observations, Atmos. Meas. Tech., 10, 2455-2475, https://doi.org/10.5194/amt-10-2455-2017, 2017.

Huang, G., Liu, X., Chance, K., Yang, K., and Cai, Z.: Validation of 10-year SAO OMI Ozone Profile (PROFOZ) Product Using Aura MLS Measurements, Atmos. Meas. Tech., 11, 17-32, https://doi.org/10.5194/amt-11-17-2018, 2018.

Kinnison, D., Tilmes, S., Levelt, P.F. Dirksen, R., Dobber, M., Voors, R., and Levelt, P.: Prelaunch characterization of the Ozone Monitoring Instrument transfer function in the spectral domain, Appl. Opt., 45, 3972–3981, doi:10.1364/AO.45.003972, 2006.

Kleipool, Q.L., Dobber, M.R., de Haan, J.F., and Levelt, P.F.: Earth surface reflectance climatology from 3 years of OMI data, J. Geophys. Res., 113, D18308, doi:10.1029/2008JD010290, 2008.

Kromminga, H., Voigt, S., Orphal, J., and Burrows, J.P.: The temperature dependence (213–293 K) of the absorption cross-sections of OClO in the 340–450 nm region measured by Fourier-transform spectroscopy, J. Photochem. Photobiol. A,157, 149-160, 2003.

Kroon, M., de Haan, J.F., Veefkind, J.P., Froidevaux, L., Wang, R., Kivi, R., and Hakkarainen, J.J., Validation of operational ozone profiles from the Ozone Monitoring Instrument, J. Geophys. Res., 116, D18305, doi:10.1029/2010JD015100, 2011.

Kühl, S., Pukite, J., Deutschmann, T., Platt, U., and Wagner, T.: SCIAMACHY limb measurements of NO_2, BrO and OClO. Retrieval of vertical profiles: algorithm, first results, sensitivity and comparison studies, Adv. Space Res., 42, 1747-1764, 2008.

Kurosu, T.P., Chance, K., and Sioris, C.E.: Preliminary results for HCHO and BrO from the EOS-Aura Ozone Monitoring Instrument, in Proc. SPIE 5652, Passive Optical Remote Sensing of the Atmosphere and Clouds IV, doi: 10.1117/12.578606 2004.

Lee, C., Richter, A., Weber, M., and Burrows, J.P.: SO_2 Retrieval from SCIAMACHY using the Weighting Function DOAS (WFDOAS) technique: comparison with Standard DOAS retrieval, Atmos. Chem. Phys., 8, 6137–6145, 2008.

Levelt, P.F., van den Oord, G.H.J., Dobber, M.R., Mälkki, A., Visser, H., de Vries, J., Stammes, P., Lundell, J., and Saari, H.: The Ozone Monitoring Instrument, IEEE Trans. Geo. Rem. Sens., 44, 1093-1101, doi:10.1109/TGRS.2006.87233, 2006.

Li, C., Joiner, J., Krotkov, N. A., and Bhartia, P. K.: A fast and sensitive new satellite SO2 retrieval algorithm based on principal component analysis: Application to the ozone monitoring instrument, Geophys. Res. Lett., 40, 6314–6318, https://doi.org/10.1002/2013GL058134, 2013.

Liao, J., Huey, L. G., Scheuer, E., Dibb, J. E., Stickel, R. E., Tanner, D. J., Neuman, J. A., Nowak, J. B., Choi, S., Wang, Y., Salawitch, R. J., Canty, T., Chance, K., Kurosu, T., Suleiman, R., Weinheimer, A. J., Shetter, R. E., Fried, A., Brune, W., Anderson, B., Zhang, X., Chen, G., Crawford, J., Hecobian, A., Ingall, E. D.: Characterization of soluble bromide measurements and a case study of BrO observations during ARCTAS, Atmos. Chem. Phys., 11, 26999-27030, https://doi.org/10.5194/acp-12-1327-2012, 2012.

Liao, J., Huey, L. G., Tanner, D. J., Flocke, F. M., Orlando, J. J., Neuman, J. A., Nowak, J. B., Weinheimer, A. J., Hall, S. R., Smith, J. N., Fried, A., Staebler, R. M., Wang, Y., Koo, J.-H., Cantrell, C. A., Weibring, P., Walega, J., Knapp, D. J., Shepson, P. B., Stephens, C. R.: Observations of inorganic bromine (HOBr, BrO, and Br2) speciation at Barrow, Alaska, in spring 2009, J. Geophys. Res. Atmos., 117, DOI:10.1029/2011JD016641, 2012

Lindström, P., and Wedin, P.-Å.: Gauss-Newton Based Algorithms for Constrained Nonlinear Least Squares Problems, Tech. Rep. UMINF-901.87, University of Umeå, 1987 (software and report available at http://plato.asu.edu/sub/nonlsq.html).

Liu, X., Bhartia, P.K., Chance, K., Spurr, R.J.D., and Kurosu, T.P.: Ozone profile retrievals from the Ozone Monitoring Instrument, Atmos. Chem. Phys. 10, 2521-2537, 2010.

Malicet, J., Daumont, D., Charbonnier, J., Parisse, C., Chakir, A., and Brion, J.: Ozone UV spectroscopy. II. Absorption cross sections and temperature dependence, J. Atmos. Chem., 21, 263-273, doi:10.1007/BF00696758, 1995.

Marquardt, D.L.: An algorithm for least-squares estimation of non-linear parameters, J. Soc. Indust. Appl. Math. 2, 431-441, 1963.

Martin, R.V., Sioris, C.E., Chance, K., Ryerson, T.B., Bertram, T.H., Wooldridge, P.J., Cohen, R.C., Neuman, J.A., Swanson, A., and Flocke, F.M.: Evaluation of space-based constraints on global nitrogen oxide emissions with regional aircraft measurements over and downwind of eastern North America, J. Geophys. Res., 111, D15308, doi:10.1029/2005JD006680, 2006.

Matveev, V., Mordechai, P., Rosen, D., Tov-Alper, D.S., Hebestreit, K., Stutz, J., Platt, U., Blake, D., and Luria, M.: Bromine oxide-ozone interaction over the Dead Sea, J. Geophys. Res. Atmos., 106, 10375-10387, 2001.

McLinden, C. A., Haley, C. S., and Sioris, C. E., Diurnal effects in limb scatter observations, J. Geophys. Res., 111, D14302, doi:10.1029/2005JD006628, 2006.

OMI Algorithm Theoretical Basis Document, Volume IV, OMI Trace Gas Algorithms, K. Chance, Ed., ATBD-OMI-04, Version 2.0, 2002.

Peterson, P. K., Simpson, W. R., and Nghiem, S. V.: Variability of bromine monoxide at Barrow, Alaska, over four halogen activation (March–May) seasons and at two on-ice locations, J. Geophys. Res.-Atmos., 121, 1381–1396, doi:10.1002/2015JD024094, 2016.

Peterson, Peter K., Simpson, William R., Nghiem, Son V.: Variability of bromine monoxide at Barrow, Alaska, over four halogen activation (March-May) seasons and at two on-ice locations, J. Geophys. Res. Atmos., 121, 1381-1396, 2016.

Platt, U.: Differential optical absorption spectroscopy (DOAS), Chem. Anal. Series, **127**, 27-83, 1994.

Platt, U. and Wagner, T.: Satellite mapping of enhanced BrO concentrations in the troposphere, Nature, 395, 6701, 486-490, 1998.

Press, W.H., Flannery, B.P., Teukolsky, S.A., and Vetterling, W.T.: Numerical Recipes, ISBN 0-521-30811-9, Cambridge University Press, 1986.

Richter, A., Begoin, M., Hilboll, A., and Burrows, J.P., An improved NO_2 retrieval for the GOME-2 satellite instrument, Atmos. Meas. Tech., 4, 1147–1159, 2011 doi:10.5194/amt-4-1147-2011.

Richter, A., Wittrock, F., Eisinger, M., and Burrows, J.P., GOME observations of tropospheric BrO in northern hemispheric spring and summer 1997, Geophys. Res. Lett., 25, 14, 2683-2686, 1998.

Rodgers, C.D.: Inverse methods for atmospheric sounding, World Scientific, 2000.

Salawitch, R.J., Canty, T., Kurosu, T., Chance, K., Q. Liang A. da Silva S. Pawson J. E. Nielsen J. M. Rodriguez P. K. Bhartia X. Liu L. G. Huey J. Liao R. E. Stickel D. J. Tanner J. E. Dibb W. R. Simpson D. Donohoue A. Weinheimer F. Flocke D. Knapp D. Montzka J. A. Neuman J. B. Nowak T. B. Ryerson S. Oltmans D. R. Blake E. L. Atlas D. E. Kinnison S. Tilmes L. L. Pan F. Hendrick M. Van Roozendael K. Kreher P. V. Johnston R. S. Gao B. Johnson T. P. Bui G. Chen R. B. Pierce J. H. Crawford D. J. Jacob: A new interpretation of total column BrO during Arctic spring, Geophys. Res. Lett., 37, L21805, doi:10.1029/2010GL043798, 2010.

Salawitch, R.J., Weinstein, D.K., Kovalenko, L.J., Sioris, C.E., Wennberg, P.O., Chance, K., Ko, M.K.W., and McLinden, C.A.: Sensitivity of ozone to bromine in the lower stratosphere, Geophys. Res. Lett., 32, 5, L05811, doi:10.1029/2004GL021504, 2005.

Schofield, R., Connor, B.J., Kreher, K., Johnston, P.V., and Rodgers, C.D.: The retrieval of profile and chemical information from groundbased UV-visible spectroscopic measurements, J. Quant. Spectrosc. Radiat. Transfer, 86, 115 – 131, 2004a.

Schofield, R., Johnston, P.V., Thomas, A., Kreher, K., Connor, B.J., Wood, S., Shooter, D., Chipperfield, M P., Richter, A., von Glasow, R., and Rodgers, C.D.: Tropospheric and stratospheric BrO columns over Arrival Heights, Antarctica, 2002, J. Geophys. Res., 111, D22310, doi:10.1029/2005JD007022, 2006.

Schofield, R., Kreher, K., Connor, B.J., Johnston, P.V., Thomas, A., Shooter, D. Chipperfield, M.P., Rodgers, C.D., and Mount, G.H.: Retrieved tropospheric and stratospheric BrO columns over Lauder, New Zealand, J. Geophys. Res., 109, D14304, doi:10.1029/2003JD00446, 2004b.

Simpson, W.R., Alvarez-Aviles, L., Douglas, T.A., Sturm, M., and Domine, F.: Halogens in the coastal snow pack near Barrow, Alaska: Evidence for active bromine air-snow chemistry during springtime, Geophys. Res. Lett., 32, L04811, doi:10.1029/2004GL021748, 2005.

Sihler, H., Platt, U., Beirle, S., Marbach, T., Kühl, S., Dörner, S., Verschaeve, J., Frieß, U., Pöhler, D., Vogel, L., Sander, R., Wagner, T.: Tropospheric BrO column densities in the Arctic derived from satellite: retrieval and comparison to ground-based measurements, Atmos. Meas. Tech., 5, 2779-2807, https://doi.org/10.5194/amt-5-2779-2012, 2012.

Simpson, W. R., von Glasow, R., Riedel, K., Anderson, P., Ariya, P., Bottenheim, J., Burrows, J., Carpenter, L. J., Frieß, U., Goodsite, M. E., Heard, D., Hutterli, M., Jacobi, H.-W., Kaleschke, L., Neff, B., Plane, J., Platt, U., Richter, A., Roscoe, H., Sander, R., Shepson, P., Sodeau, J., Steffen, A., Wagner, T., Wolff, E.: Halogens and their role in polar boundary-layer ozone depletion, Atmos. Chem. Phys., 7, 4375-4418, https://doi.org/10.5194/acp-7-4375-2007, 2007.

Sioris, C.E., Kovalenko, L.J., McLinden, C.A., Salawitch, R.J., Van Roozendael, M., Goutail, F., Dorf M., Pfeilsticker, K., Chance, K., von Savigny, C., Liu, X., Kurosu, T.P., Pommereau, J.-P., Bosch, H., and Frerick, J., Latitudinal and vertical distribution of bromine monoxide in the lower stratosphere from Scanning Imaging Absorption Spectrometer for Atmospheric Chartography limb scattering measurements, J. Geophys. Res., 111, D14301, doi:10.1029/2005JD006479, 2006.

Slijkhuis, S., von Bargen, A., Thomas, W., and Chance, K.: Calculation of undersampling correction spectra for DOAS spectral fitting, in Proceedings of the European Symposium on Atmospheric Measurements from Space, 563–569, 1999.

Spurr, R.J.D.: VLIDORT: A linearized pseudo-spherical vector discrete ordinate radiative transfer code for forward model and retrieval studies in multilayer multiple scattering media, J. Quant. Spectrosc. Radiat. Transfer, 102, 316-342, doi:10.1016/j/jqsrt.2006.05.005, 2006.

Stutz, J., Ackermann, Ralf, Fast, Jerome D., Barrie, Leonard: Atmospheric reactive chlorine and bromine at the Great Salt Lake, Utah, Geophys. Res. Lett., 29, 18-1, doi: 10.1029/2002GL014812, 2002.

Stutz, J., Thomas, J. L., Hurlock, S. C., Schneider, M., von Glasow, R., Piot, M., Gorham, K., Burkhart, J. F., Ziemba, L., Dibb, J. E., Lefer, B. L.: Longpath DOAS observations of surface BrO at Summit, Greenland, Atmos. Chem. Phys., 11, 9899-9910, https://doi.org/10.5194/acp-11-9899-2011, 2011.

Tas, E., Peleg, M., Matveev, V., Zingler, J., Luria, M.: Frequency and extent of bromine oxide formation over the Dead Sea, J. Geophys. Res., D11304, doi:10.1029/2004JD005665, 2005.

Theys, N., Van Roozendael, M., Dils, B., Hendrick, F., Hao, N., and De Mazière, M.: First satellite detection of volcanic bromine monoxide emission after the Kasatochi eruption, Geophys. Res. Lett., 36, L03809, doi:10.1029/2008GL036552, 2009.

Theys, N., Van Roozendael, M., Hendrick, F., Yang, X., De Smedt, I., Richter, A., Begoin, M., Errera, Q., Johnston, P.V., Kreher, K., and De Mazière, M.: Global observations of tropospheric BrO columns using GOME-2 satellite data, Atmos. Chem. Phys., 11, 1791-1811, https://doi.org/10.5194/acp-11-1791-2011, 2011.

Vandaele, A.C., Simon, P.C., Guilmot, J.M., Carleer, M., Colin, R.: SO2 Absorption Cross Section measurement in the UV using a Fourier Transform Spectrometer. J. Geophys. Res., 99, 25599-25605, 1994.

Vandaele, A.C., Hermans, C., Simon, P.C., Carleer, M., Colin, R., Fally, S., Mérienne, M.F., Jenouvrier, A., and Coquart, B.: Measurements of the NO_2 absorption cross sections from 42000 cm^{-1} to 10000 cm^{-1} (238-1000 nm) at 220 K and 294 K, J. Quant. Spectrosc. Radiat. Transfer, 59, 171-184, 1998.

Vandaele, A.C., Hermans, C., and Fally, S.: Fourier Transform measurements of SO_2 absorption cross sections: II. Temperature dependence in the 29 000 - 44 000 cm^{-1} (227-345 nm) region, J. Quant. Spectrosc. Radiat. Transfer, 110, 2115-2126, 2009.

Veihelmann, B. and Kleipool, Q.: Reducing Along-Track Stripes in OMI-Level 2 Products, Technical report TN-OMIE-KNMI-785, KNMI, available at http: //disc.sci.gsfc.nasa.gov/Aura/data-holdings/OMI/documents/ v003/RD08_TN785_i1_Reducing_AlongTrack_Stripes.pdf, 2006.

von Glasow, R., von Kuhlmann, R., Lawrence, M.G., Platt, U., and Crutzen, P.J.: Impact of reactive bromine chemistry in the troposphere, Atmos. Chem. Phys., 4, 2481-2497, 2004.

Wang, H., Liu, X., Chance, K., González Abad, G., and Chan Miller, C.: Water vapor retrieval from OMI visible spectra, Atmos. Meas. Tech., 7, 1901-1913, 2014.

Wang, H., González Abad, G., Liu, X., and Chance, K.: Validation of OMI total column water vapor product, Atmos. Chem. Phys., 16, 11379-11393, doi:10.5194/acp-16-11379-2016, 2016.

Weber, M., Lamsal, L.N., Coldewey-Egbers, M., Bramstedt, K., and Burrows, J.P.: Pole-to-pole validation of GOME WFDOAS total ozone with groundbased data, Atmos. Chem. Phys., 5, 1341-1355, https://doi.org/10.5194/acp-5-1341-2005, 2005.

Wilmouth, D.M., Hanisco, T.F., Donahue, N.M, and Anderson, J.G.: Fourier transform ultraviolet spectroscopy of the $A^{2}\mathrm{P}_{3/2} \neg X^{2}\mathrm{P}_{3/2}$ transition of BrO, J. Phys. Chem. A, 103, 8935-8945, 1999.

Yung, Y.L., Pinto, J.P., Watson, R.T., and Sander,S. P.: Atmospheric bromine and ozone perturbations in the lower stratosphere, J. Atmos. Sci., 37, 2, 339, 1980.

Zhao, X., Strong, K., Adams, C., Schofield, R., Yang, X., Richter, A., Friess, U., Blechschmidt, A.-M., Koo, J.-H.: A case study of a transported bromine explosion event in the Canadian high arctic, J. Geophys. Res. Atmos., 121, 457-477, doi: 10.1002/2015JD023711, 2015.

Table 1. Fitting window and parameters used to derive BrO vertical column densities

Parameter	Description/value
Fitting window	319.0 - 347.5 nm
Baseline polynomial	4th order
Scaling polynomial	4th order
Instrument slit function	Hyper-parameterization of pre-flight measurements, Dirksen *et al.*, 2006
Wavelength calibration	Spectral shift (no squeeze)
Solar reference spectrum	Chance and Kurucz, 2010
BrO cross sections	Wilmouth *et al.*, 1999, 228K
H_2CO cross sections	Chance and Orphal, 2011, 300K
O_3 cross sections	Malicet *et al.*, 1995, 218K, 295K
NO_2 cross sections	Vandaele *et al.*, 1998, 220K
SO_2 cross sections	Vandaele et al., 1994, 295K[1]
	Hermans *et al.*, 2009; Vandaele *et al.*, 2009, 295K[2]
OClO cross sections	Kromminga *et al.*, 2003, 213K
Molecular Ring cross sections	Chance and Spurr, 1997
Undersampling correction	Computed on-line, Chance *et al.*, 2005
Residual (common mode) spectrum	Computed on-line between 30ºN and 30ºS

1. Used in the current operational algorithm.
2. Used for testing sensitivity to SO_2 cross sections and will be used in the next version.

Figures and Figure Captions

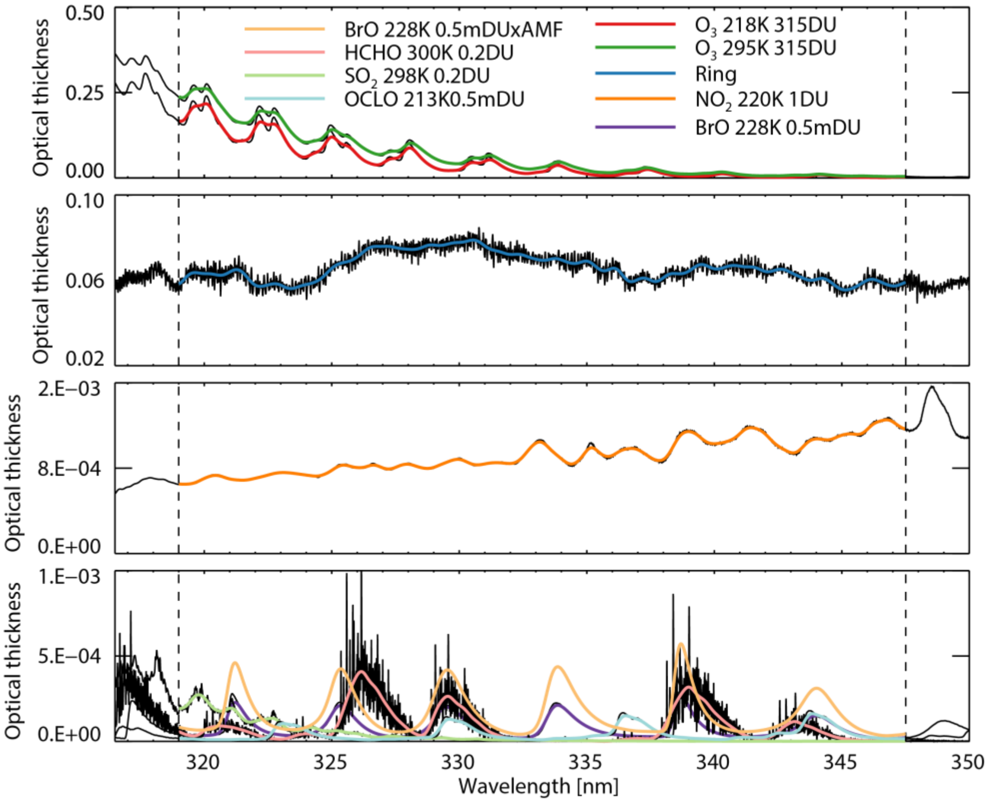

Figure 1. Cross sections used in the current operational BrO algorithm except for the SO_2 cross section at 298 K which is to be used in the next version. The black lines are the original cross sections, the color lines show the cross sections convolved with OMI slit function (which is assumed to be a Gaussian with 0.42nm full width at half maximum. The BrO cross section after multiplication with the wavelength-dependent AMFs used these parameters for the calculation: albedo = 0.05, solar zenith angle = 5.0°, and viewing zenith angle = 2.5°).

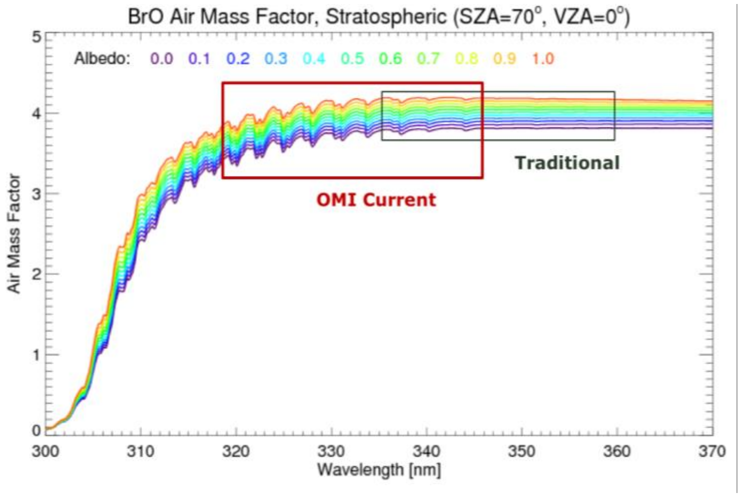

Figure 2. Wavelength- and albedo-dependent air mass factors calculated using a mostly stratospheric fixed BrO profile. The blue box shows the fitting window used in our previous versions, and the red box shows the fitting window used in the current operational algorithm.

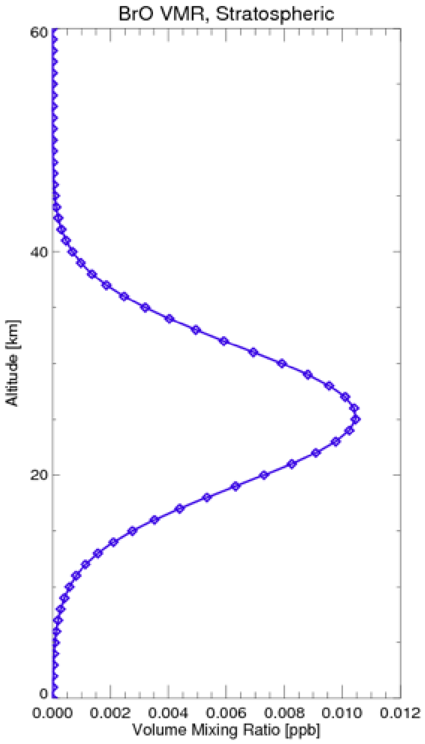

Figure 3. A mostly stratospheric vertical BrO profile used for air mass factors. Total BrO, BrO < 15 km, BrO < 10 km, and BrO < 5km are 1.55×10^{13}, 5.06×10^{12}, 1.55×10^{12}, and 2.87×10^{11}, respectively.

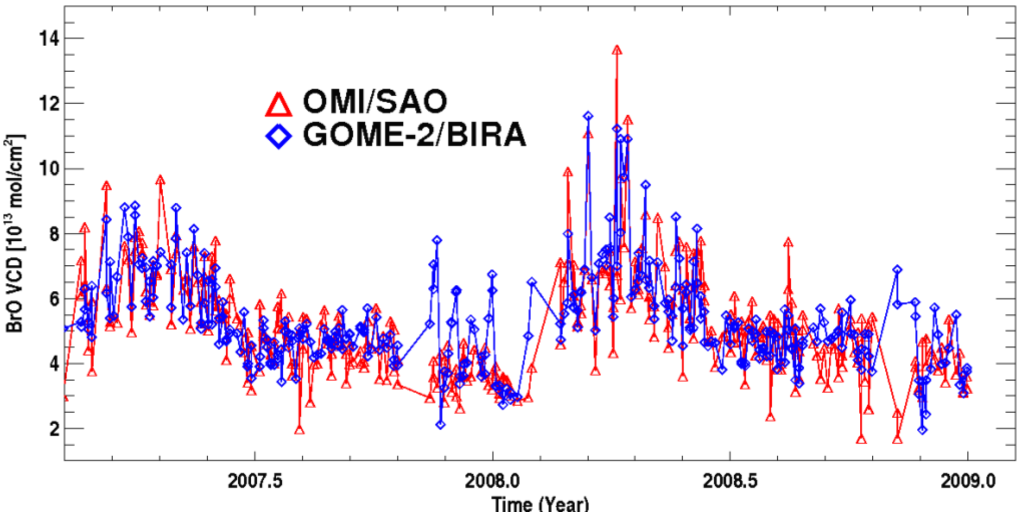

Figure 4. Time series comparison of SAO OMI (red) BrO and BIRA GOME-2 (blue) BrO VCDs from February 2007 to November 2008 using simultaneous nadir overpasses within 2 minutes between OMI and GOME-2 observations.

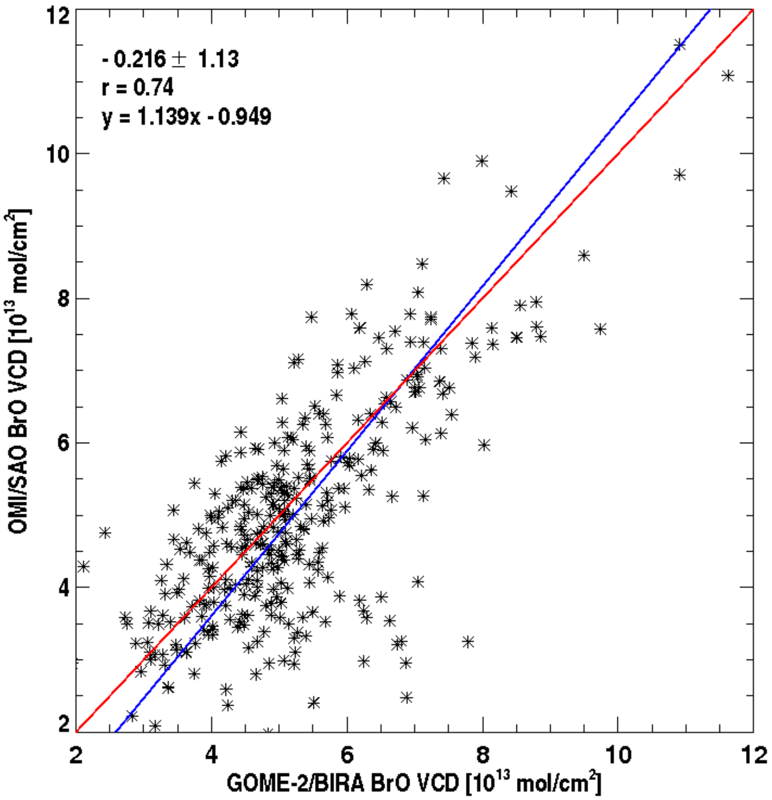

Figure 5. **Correlation and orthogonal regression of OMI and GOME-2 BrO for the data shown in Fig. 4. The legends show the mean bias and standard deviation of the differences, correlation, and the orthogonal regression.**

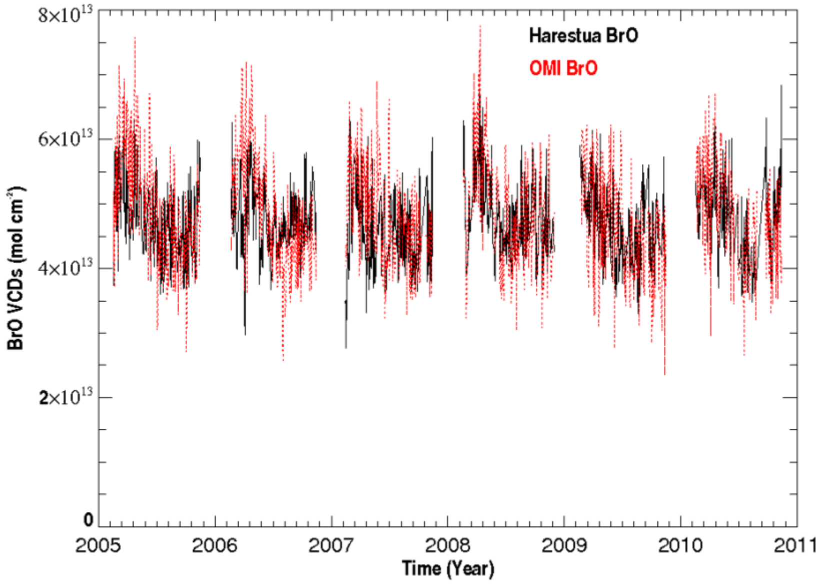

Figure 6. Time series comparison of ground-based zenith-sky total BrO (black) at Harestua, Norway and coincident SAO OMI BrO (red) from February 2005 through August 2011.

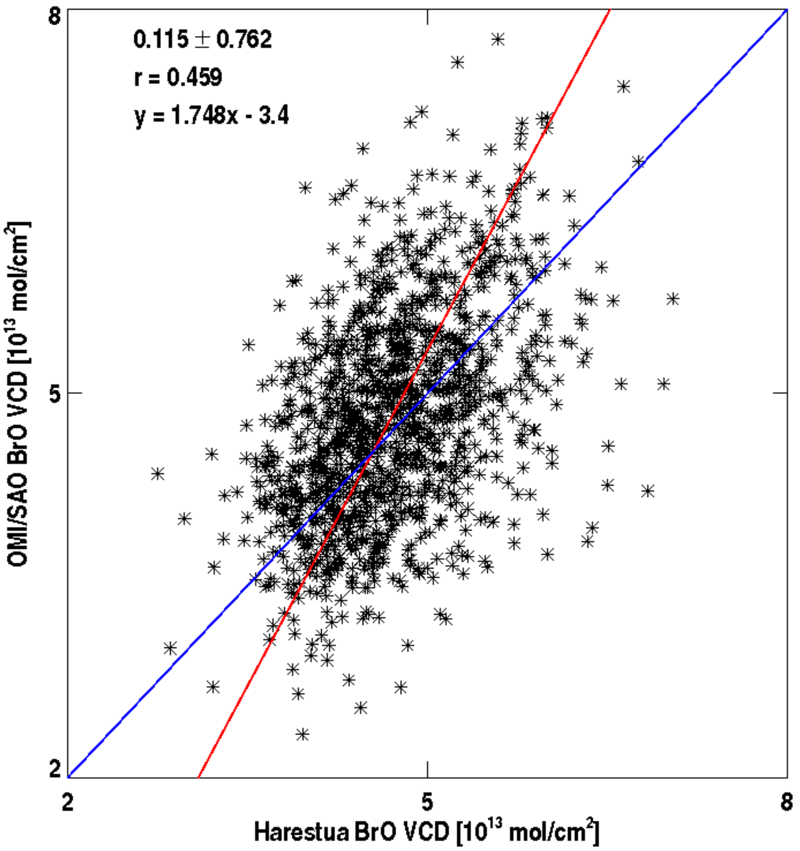

5 **Figure 7. Correlation and orthogonal regression of OMI and Harestua BrO for the data in Fig. 6. The legends show the mean biases and standard deviations of the differences, correlation, and the orthogonal regression.**

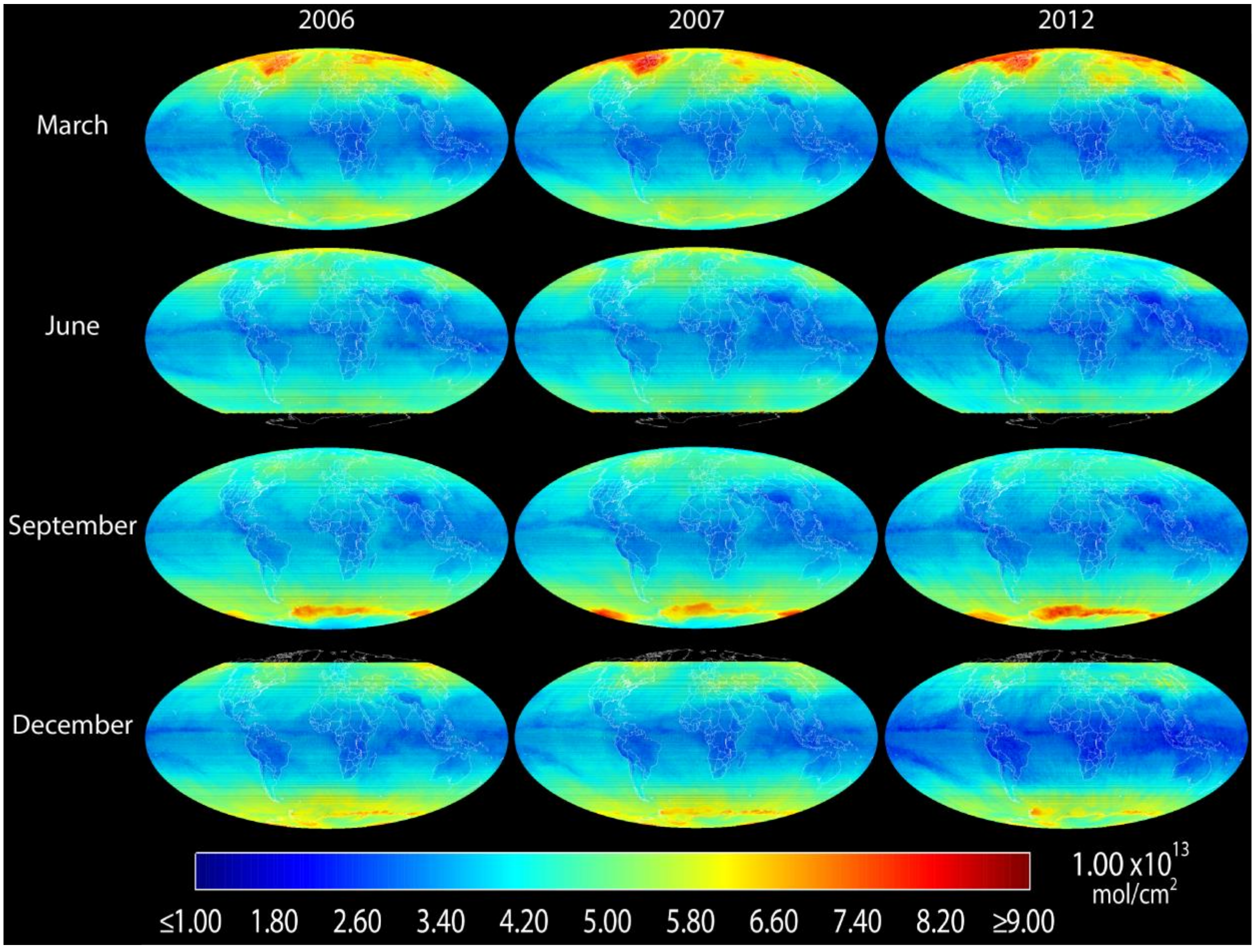

Figure 8. Global distributions of monthly mean BrO VCDs in March, June, September and December (in different rows) of 2006, 2007, and 2012 (different columns). Bromine release "explosions" during the Polar Spring months can be seen clearly.

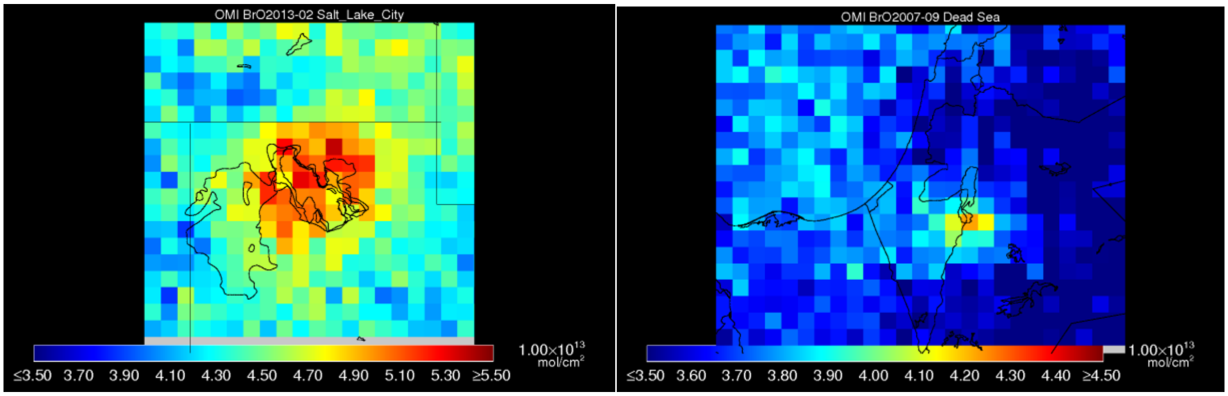

Figure 9. Monthly mean BrO VCD (left) over the U.S. Great Salt Lake for February 2013 and (right) over the Dead Sea Valley for September 2007.

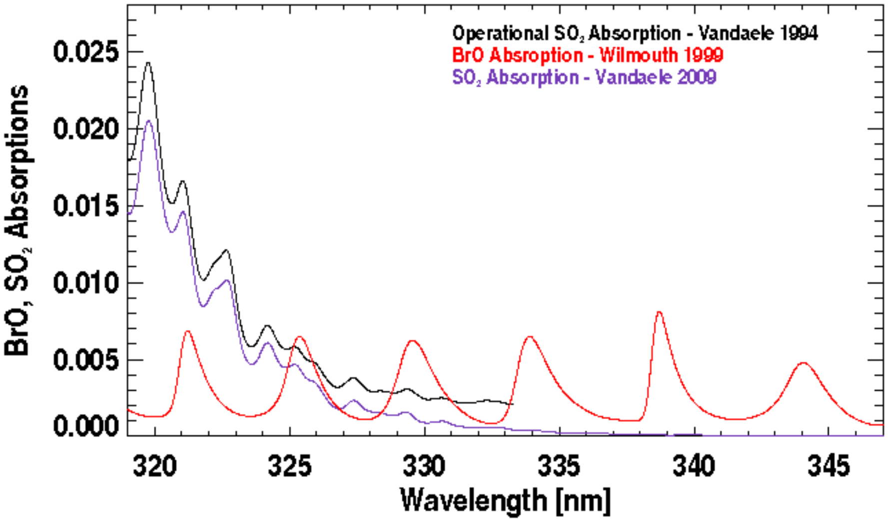

Figure 10. Comparison of BrO absorption (red) and SO$_2$ absorptions under volcanic scenarios based on cross sections used in the operational algorithm (Vandaele et al., 1994) as shown in black and the recent laboratory cross sections (Vandaele et al., 2009) as shown in purple. For BrO, a SCD of 1.0×10^{14} molecules cm^{-2} is assumed; for SO$_2$, a SCD of 15 Dobson Units (i.e., 4.03×10^{17} molecules cm^{-2}) is assumed. Cross sections have been convolved with OMI slit function (which is assumed to be a Gaussian with 0.42nm full width at half maximum).

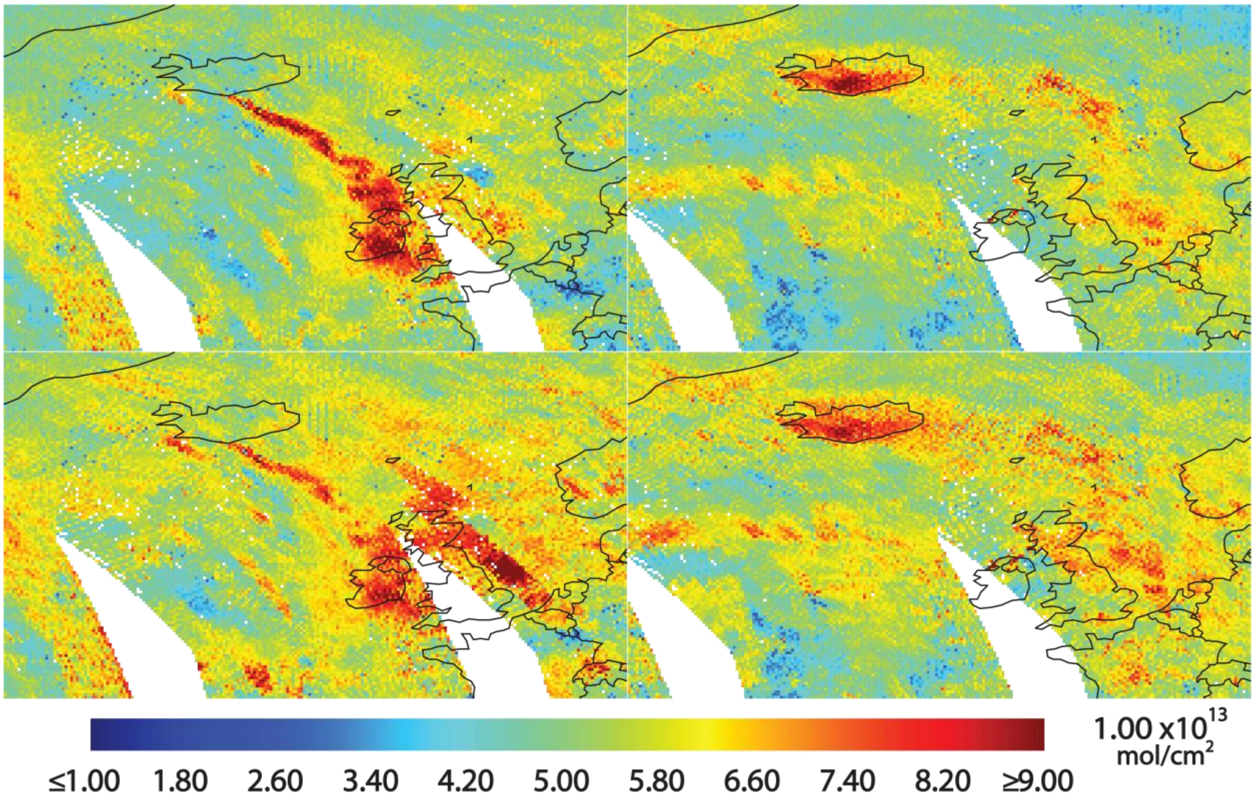

Figure 11. Daily average BrO VCDs from Eyjafjallajökull on May 5 and 17, 2010 produced using (top) the operational SO_2 cross sections and (bottom) the Vandaele et al. (2009) SO_2 cross sections.